Synthetic Dual-Doppler Analysis of a Winter Mesoscale Vortex

NEIL F. LAIRD

Atmospheric Environment Section, Illinois State Water Survey, Illinois Department of Natural Resources, Champaign, Illinois

L. JAY MILLER

Mesoscale and Microscale Meteorology Division, National Center for Atmospheric Research, Boulder, Colorado

DAVID A. R. KRISTOVICH

Atmospheric Environment Section, Illinois State Water Survey, Illinois Department of Natural Resources, Champaign, Illinois

(Manuscript received 15 March 2000, in final form 26 June 2000)

ABSTRACT

This article presents a detailed examination of the kinematic structure and evolution of the 5 December 1997 winter mesoscale vortex in the vicinity of Lake Michigan using the synthetic dual-Doppler (SDD) technique. When such a mesoscale event propagates a distance large enough that the viewing angle from a single-Doppler radar changes by about 30° and the circulation is sufficiently steady during this time period, then the SDD method can reveal reliable details about the circulation. One such detail of the observed vortex was a pattern of convergence and divergence associated with radial bands, where heavier snowfall was located. Another was the steadiness and vertical coherence of the derived vorticity and convergence patterns within the cyclonic circulation.

On 5 December 1997, the observed reflectivity field remained remarkably steady for nearly 2.5 h as the vortex moved southeastward allowing for the application of the SDD technique. The reflectivity field exhibited a pronounced asymmetric convective structure with at least three well-defined, inward-spiraling radial snowbands, and a distinct weak-reflectivity region or ''eye'' near the center of cyclonic circulation. The SDD results showed the vortex circulation was composed of a combination of rotation on the meso-β scale and convergence on the meso-γ scale associated with the embedded radial snowbands. Vertical profiles of derived meso-β-scale, area-mean convergence and vorticity suggest that this winter vortex was likely a warm-core system, similar to both tropical cyclones and polar lows.

1. Introduction

The Great Lakes often function as a source of atmospheric heat and moisture in the winter. Their modifying effect on the planetary boundary layer, mesoscale circulations, and precipitation intensity and distribution is especially significant and complex during arctic cold-air outbreaks. Winter mesoscale vortices are one of several types of coherent mesoscale circulations that occur in the Great Lakes region during winter (e.g., Hjelmfelt 1990). Here we have defined winter mesoscale vortices as cyclonic circulations originating in the Great Lakes region and having a horizontal scale less than an individual lake.

The majority of winter mesoscale vortices have been observed using visible satellite imagery. For example, Forbes and Merritt (1984) found 14 cases of mesoscale vortices over the western Great Lakes in the years 1978–82. Pitts et al. (1977) observed several simultaneous meso-γ vortices embedded within a single land-breeze convergence zone using imagery from Skylab. Pease et al. (1988) used high-resolution Landsat imagery to examine a vortex that formed over southern Lake Michigan. Using Geostationary Operational Environmental Satellite imagery, Laird (1999) observed coexisting meso-β vortices over Lakes Superior, Huron, and Michigan during a late autumn lake-effect event. Fewer observations of winter mesoscale vortices have been documented using weather radars. Sheffield (1964) and Peace (1966) used WSR-57 radars to observe winter mesoscale

Corresponding author address: Neil F. Laird, Atmospheric Environment Section, Illinois State Water Survey, 2204 Griffith Drive, Champaign, IL 61820.
E-mail: n-laird@uiuc.edu

vortices over Lakes Erie and Ontario. Schoenberger (1986a) completed dual-Doppler radar syntheses to examine circulations of a series of meso-γ vortices that developed along a land-breeze convergence zone over Lake Michigan.

The focus of this study will be a winter mesoscale vortex that was observed in the early morning hours of 5 December 1997 over Lake Michigan and southwestern Lower Michigan. As the vortex propagated inland, there were rapid increases in the snowfall intensity over the region. We use the synthetic dual-Doppler (SDD) technique (Bluestein and Hazen 1989; Klimowski and Marwitz 1992) to determine the horizontal wind field from single-Doppler radial velocity measurements collected by the National Weather Service (NWS) Grand Rapids, Michigan (KGRR), Weather Surveillance Radar-1988 Doppler (WSR-88D). Previous investigations have found that useful horizontal wind fields can be recovered from single-Doppler data using the SDD technique.

Peace et al. (1969) were among the first to suggest that single-Doppler radar data collected during two time periods could be used to retrieve the horizontal wind field associated with a radar echo. The viability of the SDD technique and its sensitivity to several important parameters (e.g., time between the two volume scans, storm advection velocity) have been examined by Klimowski and Marwitz (1992) and Bluestein et al. (1994). Despite some limitations of the SDD technique, such as the position and propagation of the storm with respect to the radar and the assumption of a steady-state velocity field, it has proven useful for several mesoscale investigations. However, nearly all of the studies using SDD analysis have examined summer mesoscale convective systems (e.g., Bluestein et al. 1994), thunderstorm outflows and squall lines (e.g., Klimowski and Marwitz 1992), or tropical cyclones (e.g., Bluestein and Hazen 1989). Miller et al. (1996) is the only study of which the authors are aware that has used SDD analyses, in combination with an array of other mesoscale observations, to document a winter weather event (i.e., a shallow, dry arctic front).

We will use the results of the SDD analyses and an examination of the atmospheric environment to help understand the kinematic structure and evolution of the 5 December winter mesoscale vortex. Schoenberger (1986a) presented the only other study addressing the kinematic structure of winter mesoscale vortices. He used dual-Doppler radar measurements to examine a series of meso-γ vortices, with a spacing of about 20 km, which developed along a north–south Lake Michigan midlake snowband on 19 December 1983. While the vortices described by Schoenberger (1986a) had a smaller horizontal scale ($\sim$10 km diameter) and were shallower ($\sim$2 km depth) than the 5 December 1997 vortex, there are some similarities in the structure of the vortices from the two cases. This article examines the performance of the SDD technique for the 5 December 1997 event, the atmospheric environment in which the vortex developed, and the structure and evolution of the vortex as determined from the KGRR radar measurements.

2. Data

Data used for this study were collected during the Lake-Induced Convection Experiment (Lake-ICE; Kristovich et al. 2000), conducted in the Great Lakes region during the winter of 1997/98. Research datasets from Lake-ICE used in this investigation include measurements collected by three National Center for Atmospheric Research (NCAR) Integrated Sounding Systems (ISS) deployed in the vicinity of Lake Michigan. The ISS obtained surface meteorological measurements and vertical profiles of high-resolution wind, temperature, and humidity. Additional datasets used include NWS surface station and sounding observations throughout the Great Lakes region.

The KGRR radar collected the primary dateset used in this study. Doppler radar data for the 5 December 1997 case were archived at level II (base data). Archived data include radar equivalent reflectivity factor (hereafter called reflectivity), radial velocity, and spectrum width. The scan strategy used by the KGRR radar allowed volumes to be completed at 10-min time intervals with five constant elevation angles (i.e., 0.5°, 1.5°, 2.5°, 3.5°, 4.5°). The S-band (10.0–11.1-cm wavelength, 2700–3000 MHz) WSR-88D radar has a beamwidth of 0.925° and transmits with a nominal peak power output of 750 kW. On 5 December 1997, KGRR operated in clear-air mode. In this mode, the radar has a pulse duration of 4.7 μs for pulse repetition frequencies between 318 and 452 Hz for reflectivity measurements and a pulse duration of 1.57 μs for pulse repetition frequencies between 318 and 1304 Hz for velocity measurements. These values translate to a pulse length of 1.41 and 0.47 km for reflectivity and radial velocity measurements, respectively. Since a pulse radar cannot resolve two targets lying along the same bearing from the radar and separated by a radial distance of less than half the pulse length, the corresponding along-beam resolutions are approximately 0.71 and 0.24 km. Further details about the WSR-88D radar can be found in Crum et al. (1993).

Figure 1 shows locations of the KGRR radar site, the Lake-ICE ISS sites in the vicinity of Lake Michigan, NWS surface and sounding stations, and the track of the mesoscale vortex determined from KGRR measurements. The location of the vortex and its propagation speed and direction allowed it to be observed by KGRR for nearly 4.5 h. Figure 2 shows the observed reflectivity and radial velocity fields at the 0.5° elevation angle at 1013 and 1113 UTC. The vortex is well defined in both the reflectivity field with several inward-spiraling radial snowbands and radial velocity field with a distinct couplet of inbound and outbound velocities (circled region) near the vortex center.

The radar reflectivity and radial velocity fields were

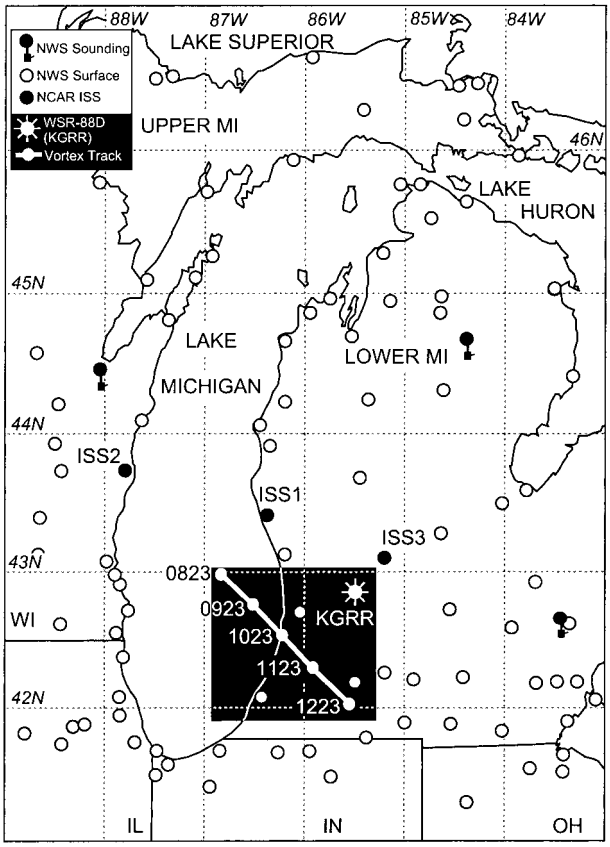

FIG. 1. Map showing the Grand Rapids, MI (KGRR), WSR-88D radar site; the Lake-ICE NCAR ISS sites in the vicinity of Lake Michigan; NWS surface station and sounding locations; and the track of the mesoscale vortex determined from KGRR measurements. The black region shows the synthetic dual-Doppler analysis area. The position of the vortex center is denoted at several times (UTC).

interpolated to a Cartesian grid using the NCAR/Mesoscale and Microscale Meteorology Division (MMM). Sorted Position Radar Interpolation program (SPRINT; Mohr and Vaughan 1979; Miller et al. 1986). Data were interpolated using a horizontal and vertical resolution of 2.0 and 0.5 km, respectively. Synthetic dual-Doppler syntheses of the horizontal winds, calculation of derived fields, and creation of graphical displays were done with the NCAR/MMM Custom Editing and Display of Reduced Information in Cartesian space program (CEDRIC; Mohr et al. 1986). A linear least squares filter over one-gridpoint radius was applied to the synthesized winds to reduce the effects of random errors in the radar velocity data.

3. Synthetic dual-Doppler technique

a. Synthetic dual-Doppler methodology

The SDD technique was first described by Peace et al. (1969) when pioneering researchers were developing new interpretative techniques to relate radial velocity measurements obtained from pulse Doppler radars to their associated horizontal wind fields. Kraus (1974) is considered the first to implement the SDD technique by using single-Doppler measurements to study a convective thunderstorm. The technique has proven useful for several mesoscale investigations (e.g., Bluestein and Hazen 1989; Miller et al. 1996), provided the wind field remains nearly steady state in the reference frame of the storm and the storm motion results in a significant change in the radar viewing angle with time. A brief review of the SDD technique is provided for completeness with more detailed descriptions given by Klimowski and Marwitz (1992) and Bluestein and Hazen (1989).

The SDD technique uses radial velocity measurements from a single radar that observes a storm, in our case a mesoscale vortex, at two time periods. Figure 3 shows a schematic of the SDD geometry for (panel a) radar-relative and (panel b) vortex-relative coordinates. In radar-relative coordinates, the vortex is first viewed at $t - \Delta t/2$, where Δt is the time separation of the two radar volumes used for the SDD analysis and t is the time of the SDD retrieval. At some later time, $t + \Delta t/2$, the vortex has moved a distance, d, to a new location with a change in the radar viewing angle, β, from the radar to the storm. In Fig. 3, d is analogous to the radar baseline in a conventional dual-Doppler system. Using radial velocity measurements from these two time periods, an SDD horizontal wind field can be retrieved for an intermediate time period, t, when the vortex was located at an intermediate distance, $d/2$. The geometry of the vortex-relative coordinates in Fig. 3b is identical to a conventional dual-Doppler (i.e., two radar) system that is viewing a single storm during the same time period. However, when using the SDD technique with a single radar it is necessary to shift the position of the radar a distance $d/2$ for both time periods by using the storm propagation velocity. Figure 3b shows that using data collected at two time periods and shifting the radar position can in essence allow a single radar to obtain measurements of the vortex from two viewing geometries at an intermediate time and location.

There are several limiting factors that are important to examine when considering the use of the SDD technique. These are the (a) storm propagation velocity; (b) change in the viewing angle from the radar to the storm, β; and (c) change of the wind field in the reference frame of the storm. In order for the SDD technique to be used the storm must have some propagation velocity. The horizontal wind field for motionless systems cannot be retrieved using the SDD method. The velocity and location of the storm with respect to the radar are important factors when considering β. Bluestein et al. (1994) state that a minimum β of 30° is usually necessary to resolve the wind field associated with convective phenomena accurately, while a minimum β of 20° may be sufficient for accurately determining the mesoscale aspects of the wind field. Therefore, it is necessary for the storm to propagate with a constant

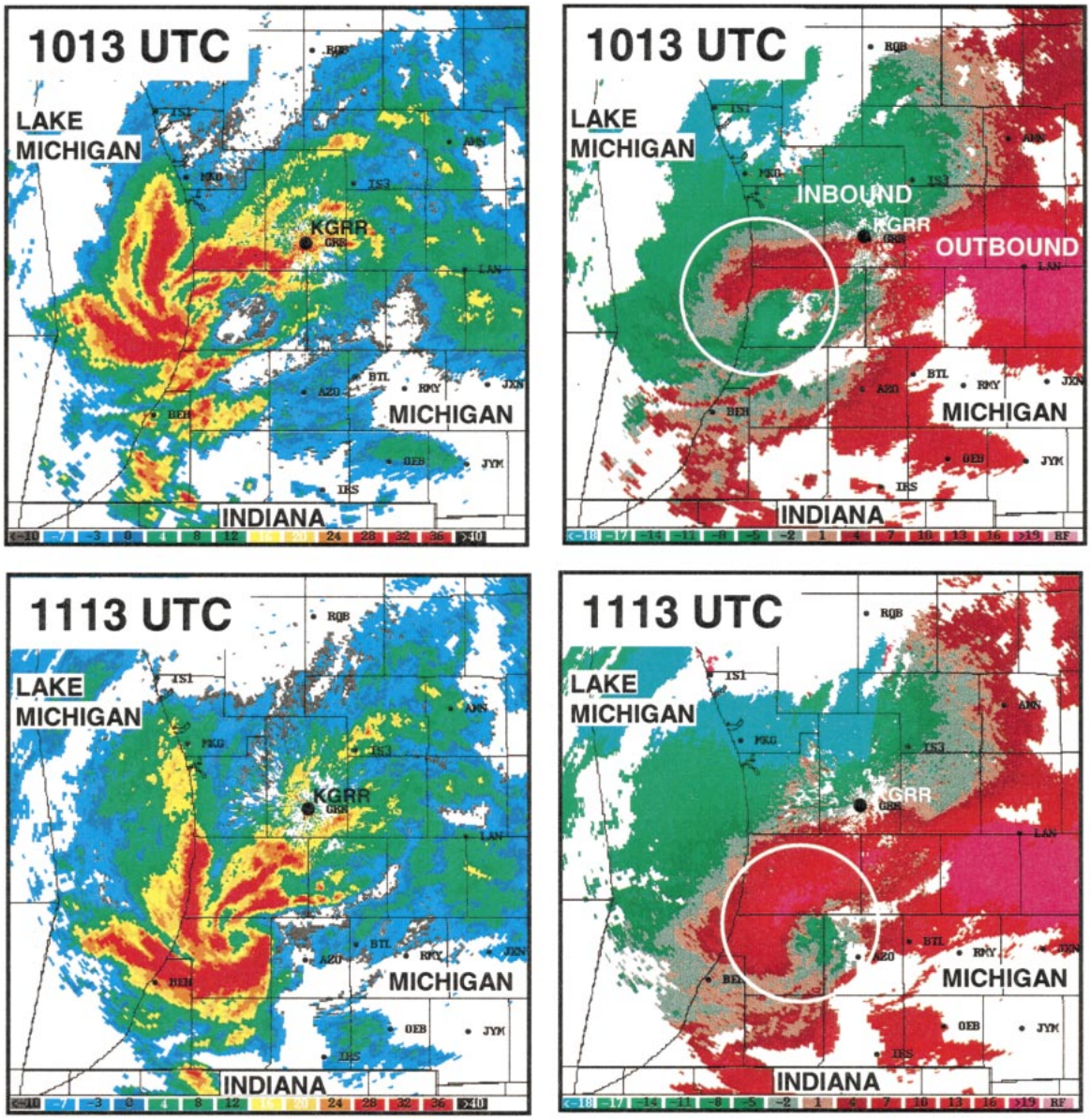

FIG. 2. (left column) Radar reflectivity and (right column) radial velocity on the 0.5° elevation level at 1013 and 1113 UTC. Reflectivity is shown from <10 to 40 dBZ at 4-dBZ intervals. Circle on radial velocity panels designates the inbound (green) and outbound (red) radial velocity couplet in the region of the vortex.

direction to the side of the radar, as in Fig. 3a, and have a speed that will reduce the time separation of the radar volumes, but still meet the minimum criteria of β stated above. Additionally, it is necessary for the structure of the wind field in the reference frame of the storm to undergo minimal change because the SDD technique invokes a steady-state assumption. This is perhaps the weakest aspect of the SDD technique and needs to be examined thoroughly for each event considered, thereby being a major limiting factor in the general utilization of the SDD method. The limiting factors of the SDD technique are addressed and the SDD geometry is determined for the 5 December 1997 vortex in the remainder of this section

It is important to accurately determine the propagation velocity and location relative to the radar for each storm examined using the SDD method. For the vortex event, an objective spatial correlation method was used to estimate the vortex speed and direction based on 18 radar volumes. The spatial correlation of interpolated reflectivity fields at the 2.0-, 2.5-, 3.0-, and 3.5-km height levels separated by 30 min in time were used within a 125 km $\times$ 125 km region (see Fig. 1) encompassing the vortex. For example, the 2.0-km reflectivity

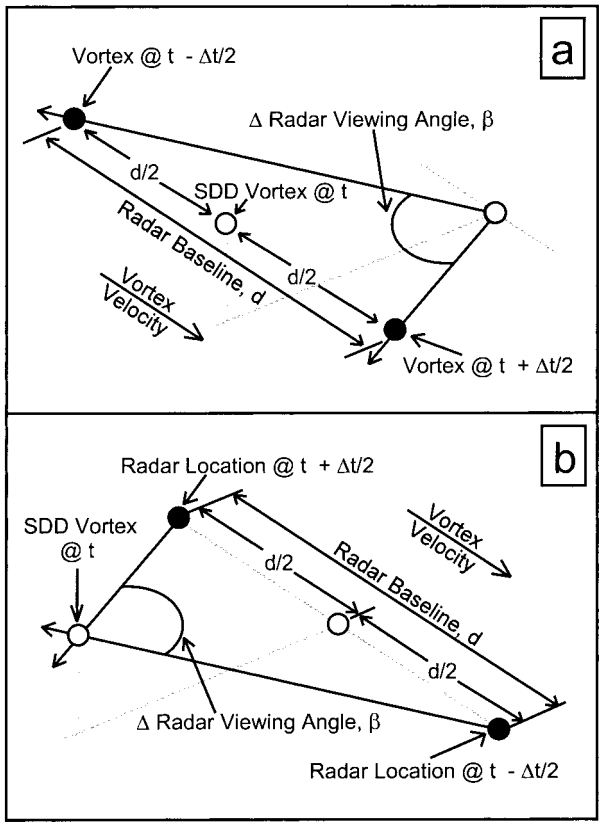

FIG. 3. Schematic diagrams of the SDD geometry for (a) radar-relative and (b) vortex-relative coordinates. Here, Δt is the time separation of the two radar volumes used for the SDD analysis and t is the time of the SDD retrieval. The distance d is analogous to the radar baseline in a conventional dual-Doppler system. The solid circles represent (a) the observed vortex locations and (b) the shifted radar locations. The open circles denote the location of the radar and the SDD retrieved vortex.

field at 1023 UTC was spatially correlated with the 2.0-km reflectivity field at 1053 UTC. The horizontal components of the vortex motion were determined from the location of the maximum correlation. Figure 4 shows an example of two reflectivity fields at 2.0 km, the spatial correlation field, and the vortex motion vector. The maximum correlation coefficients were consistently greater than 0.75 for reflectivity fields separated by 30 min for volumes compared between 0913 and 1203 UTC. The results from 60 spatial correlations showed the average and standard deviation of the vortex propagation was 8.4 ± 1.2 m s^{-1} toward $142 \pm 6°$.

Other objective methods of calculating the motion of a mesoscale field, such as the method presented by Gal-Chen (1982), have been used when advective motions are difficult to determine. For our particular event, the distinct features in the reflectivity field associated with the vortex (Figs. 2 and 3) and the small standard deviations of the estimated propagation speed (± 1.2 m s^{-1}) and direction ($\pm 6°$) created a situation that did not demand the use of other objective techniques. Bluestein and Hazen (1989) and Klimowski and Marwitz (1992) suggest that SDD results may not be sensitive to small variations in the estimated propagation velocity that cause translation errors less than about 3–6 km over the SDD time interval. Using our standard deviations of ± 1.2 m s^{-1} and $\pm 6°$ as a basis, translation errors of 0.5 and 1.8 km would occur with a 1.2 m s^{-1} and 6° deviation and 2.4 m s^{-1} and 12° deviation, respectively, for Δt equal to 1 h. It is worth noting that both of these estimated translation errors are smaller than the horizontal grid spacing used for our radar interpolation.

Since the SDD method assumes the wind field remains in a steady state during the time period Δt, it was important to closely examine the rate of change of the vortex structure. Previous investigations (e.g., Miller et al. 1990) have shown the steadiness of a storm can be estimated by comparing the reflectivity field at several different time periods, thereby providing an indication of the steadiness of the velocity field within a meteorological echo. The maximum spatial correlation coefficients having values consistently larger than 0.75 and the slowly evolving nature of the reflectivity and radial velocity fields from 0913 to 1203 UTC suggest that the vortex was in an approximate steady state for several hours. Results from an analysis to further examine the steadiness of the vortex are shown in Fig. 5. The reflectivity field at heights between 1.0 and 4.0 km for 15 radar volumes (i.e., 0943–1203 UTC) were compared to the corresponding reflectivity field at 0933 UTC. The time and position of the reflectivity fields from the 15 volumes were shifted to 0933 UTC using an average vortex propagation speed of 8.4 m s^{-1} at all height levels. This allowed for a direct comparison of the overlaid reflectivity fields assuming the average vortex propagation velocity was correct and no rotation of reflectivity features about the vortex center existed. The absolute value of the average difference in reflectivity, $|\overline{\Delta\ \mathrm{dB}Z}|$, between each time period and 0933 UTC at each height is shown in Fig. 5a. The reflectivity field appeared to change most rapidly at lower levels (i.e., below 1.5 km) and near echo top where fewer radar returns were available (i.e., 4.5 km; not shown). A portion of the changes at the 1.0- and 1.5-km levels was likely a consequence of slightly slower propagation speeds (i.e., a reduction of ≤ 0.6 m s^{-1}) of the reflectivity echoes at these levels. Using the average propagation speed of 8.4 m s^{-1}, the structure of the reflectivity field from 2.0 to 4.0 km remained remarkably steady for the 2.5-h time period, suggesting the vortex structure did not undergo substantial changes.

Figure 5b shows the standard deviation of the difference field, $\sigma(\Delta\ \mathrm{dB}Z)$, for each time and height. The increase of σ with time suggests several things may have occurred: (a) smaller-scale convective elements changed, (b) the dominant radial snowbands associated with regions of higher reflectivity changed position with respect to the vortex center during the period, and/or (c) the vortex propagation velocity was not accurate.

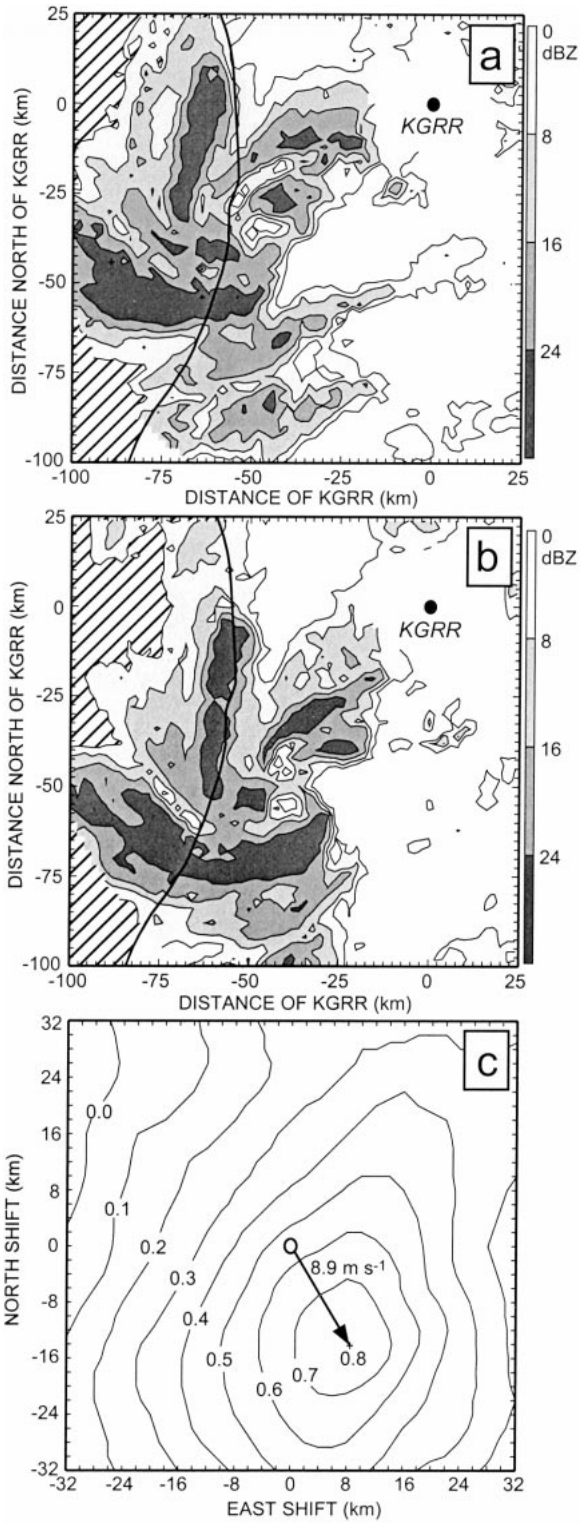

FIG. 4. Radar reflectivity fields at 2.0 km from (a) 1023 UTC and (b) 1053 UTC and (c) the mesoscale vortex motion vector determined from the spatial correlation field. The correlation field is contoured at intervals of 0.1 with a maximum of 0.8. Thick solid line in (a) and (b) shows location of Lake Michigan shoreline.

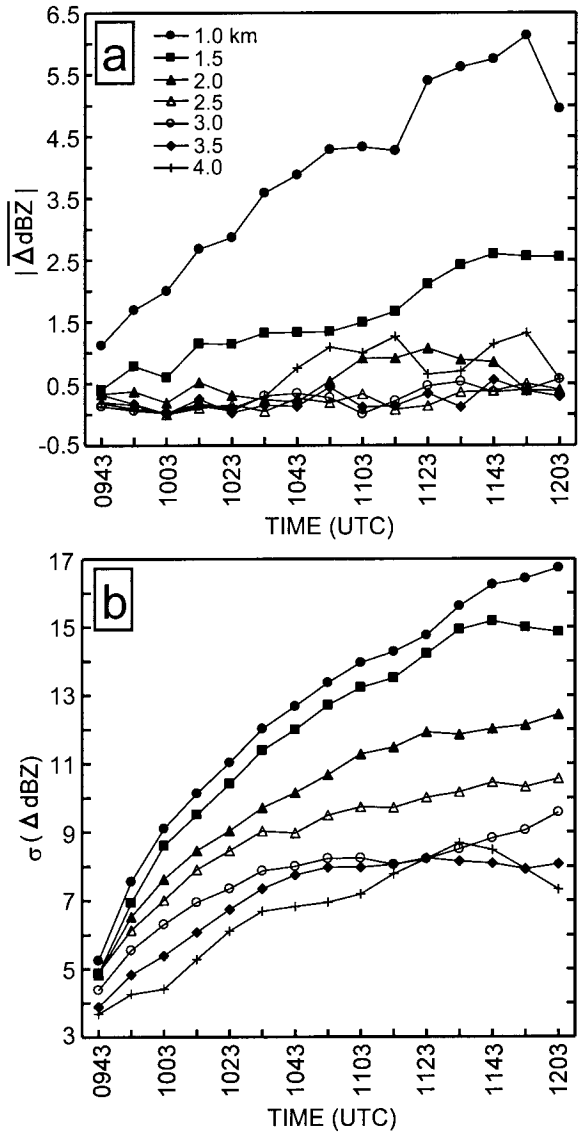

FIG. 5. (a) The absolute value of the average difference in reflectivity, $|\overline{\Delta\ \mathrm{dBZ}}|$, between radar measurements at each time period and 0933 UTC. (b) The standard deviation of the reflectivity difference field, $\sigma(\Delta\ \mathrm{dBZ})$. Curves are shown for heights from 1.0 to 4.0 km for 15 radar volumes.

Inspection of the positions of the three dominant radial snowbands showed a slow rotation (<1 m s^{-1}) around the vortex center. This along with any inaccuracy in the vortex propagation velocity likely resulted in an increase of both $|\overline{\Delta\ \mathrm{dBZ}}|$ and $\sigma(\Delta\ \mathrm{dBZ})$ with time. Although the consistent nature of the reflectivity field does not directly demonstrate that the wind field did not change during the period, it does provide strong supporting evidence that the kinematic structure associated with the vortex may not have undergone substantial changes. The SDD wind analyses shown in section 5 will demonstrate that the wind field did in fact remain quasi-steady with

respect to the vortex during the 2.5-h observation period.

Klimowski and Marwitz (1992) demonstrated the dependency of the time separation between radar volumes, Δt, on the quality of the SDD-retrieved wind field. Their analyses showed that the similarity between SDD and conventional dual-Doppler winds for the same time period significantly decreased when values of Δt were greater than 20 and 59 min for their gust front and thunderstorm cases, respectively. The time separation of the KGRR radar volumes chosen for our SDD syntheses was based on the vortex propagation speed, distance of the vortex from the radar, and the requirement that the central angle from the radar to the vortex change by 30°. The 30° requirement was used so details of the vortex structure and evolution could be examined. The vortex remained at a distance between 60 and 80 km from the radar for nearly 3 h and propagated with an average speed of 8.4 m s^{-1} toward the southeast (142°). The required Δt for this study was found to be approximately 60 min. For example, a synthesis at 1023 UTC was derived from KGRR volumes collected at 0953 and 1053 UTC. The time separation of the radar volumes and the propagation speed of the vortex provided a radar baseline of 30.2 km for the SDD analyses, which is similar to typical dual-Doppler radar baselines (e.g., 20–50 km). Since KGRR volumes were collected at 10-min time intervals, 12 SDD syntheses could be developed from 18 radar volumes between 0913 and 1153 UTC.

b. Single-Doppler estimation of synthetic dual-Doppler reliability

Several previous investigations using the SDD technique have compared single-Doppler retrieved wind fields with dual-Doppler wind fields (i.e., synthesized using two radars) to estimate the errors associated with their SDD analyses (e.g., Klimowski and Marwitz 1992; Bluestein et al. 1991). The conventional dual-Doppler winds have traditionally been taken to represent the actual wind field despite the presence of errors associated with each synthesis method (Doviak et al. 1976). Other studies have used different validation methods when dual-Doppler measurements were not available. For example, Bluestein et al. (1994) measured the accuracy of the SDD analysis by comparing results with wind profiles obtained from an NWS sounding and velocity–azimuth display (VAD) analyses for their 13 June 1989 case. To determine the validity of the SDD syntheses for the 5 December 1997 vortex, we compared the radial velocity field resampled from the SDD synthesized winds and the observed radial velocity field measured at the intermediate time. For example, the observed radial velocity field at 1023 UTC was compared with a resampled radial velocity field from the 1023 UTC SDD synthesis. It should be reiterated that the 1023 UTC SDD synthesis had been derived from the 0953 and 1053 UTC radar volumes. The resampling of the radial velocity field from the SDD winds at each height level was performed using CEDRIC and the comparison with the observed radial velocity field was completed on the Cartesian radar synthesis grid. Since the SDD winds were obtained from radar volumes ±30 min of the observed time period, this approach provided a source of data (i.e., observed radial velocity field) not used in that particular SDD wind synthesis. Therefore, this analysis method provided an estimate of the potential errors associated with each SDD synthesis. This method was used for all analyzed height levels and time periods.

Figures 6a and 6b show the 1053 UTC 2-km-level radial velocity field observed by KGRR and the SDD-derived radial velocity field. Both the observed and SDD radial velocity fields clearly show the inbound and outbound velocities associated with the vortex and are visually very similar. Figure 6c compares the observed and SDD radial velocities using linear least squares regression analysis. The two radial velocity fields are highly correlated (correlation coefficient = 0.99) with little scatter (standard error = 0.49) for the 2.0-km level at 1053 UTC. Figure 7 shows the correlation coefficients (panel a) and standard errors (panel b) over the depth of the vortex for 20 syntheses (0853–1203 UTC) within a 125 km × 125 km region. Correlation coefficients ranged from 0.925 to 0.995 and standard errors were between 0.8 and 1.8 below 2.0 km and <0.9 above 2.0 km. The large values of standard error at the 1.0- and 1.5-km levels represent the scatter in radial velocities due to the examination of SDD winds close to the radar baseline. When only the region surrounding the vortex was examined and the area close to the radar was excluded from the analyses, standard errors decreased at the lower levels. This finding is not surprising since the normalized geometric error in dual-Doppler synthesized winds are large near the radar baseline where both radars are approaching the measurement of the same component of the wind (e.g., Lhermitte and Miller 1970; Miller and Kropfli 1980). The radar echo associated with the vortex has a maximum depth of nearly 4.5 km. The more variable and often lower correlation coefficients at 3.5 km are consistent with the more rapidly changing structure closer to the radar echo top.

In general, there are only small differences in the magnitude of the observed and SDD radial velocities. For example, Fig. 6d shows the largest differences in the 2-km radial velocities at 1053 UTC are located near the vortex center where a small region of observed outbound velocities are about 2 m s^{-1} larger than SDD velocities. The magnitudes of the errors associated with the SDD analyses were found to be similar to the variability in the observed radial velocities, based on spectrum width measurements (not shown), and seem to be only slightly larger than velocity errors typically associated with conventional dual-Doppler syntheses (e.g., Doviak et al. 1976). The 2-km relative wind field (i.e., mean wind subtracted, $u = 5.2$ m s^{-1}, $v = -6.6$ m s^{-1}) at 1053 UTC is shown in Fig. 6b. The cyclonic rotation

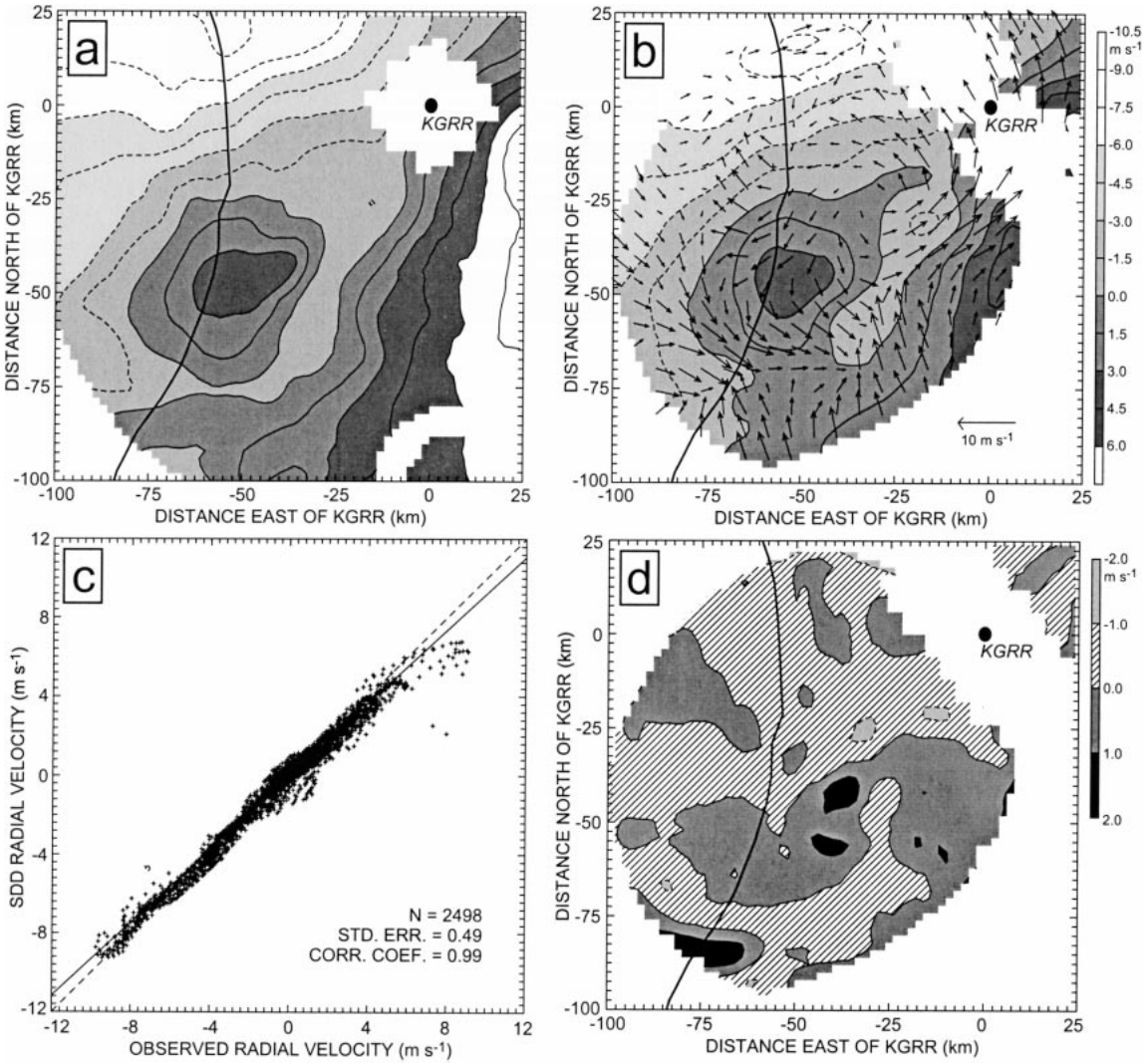

FIG. 6. (a) The 1053 UTC 2-km observed radial velocity field and (b) the SDD-derived radial velocity and relative wind fields. (c) Linear least squares regression analysis comparing the observed and SDD radial velocities. The solid line shows the 1:1 correlation line. The calculated relation is shown with the dashed line. In addition, the number of data points, standard error, and correlation coefficient are shown. (d) The difference field of the observed and SDD 2-km radial velocity fields at 1053 UTC. Thick solid line in (a), (b), and (c) shows location of Lake Michigan shoreline.

about the vortex center and convergence (divergence) linked to the deeper (shallower) radial snowbands is well defined in the relative wind field.

Previous studies have provided cautionary statements about the use of SDD analyses to examine the detailed structure of mesoscale systems. Bluestein et al. (1994) suggest that although SDD analysis can be suitable for determining the overall type of wind field in a mesoscale convective system, it may not be suitable for quantitative estimates of kinematic quantities such as horizontal divergence, thermodynamic retrieval, or for initializing numerical models. Klimowski and Marwitz (1992) concluded that the use of SDD analyses may be questionable for detailed diagnostic studies, but that further investigations should be undertaken to determine the viability of the SDD technique in recovering derived parameters such as divergence, vorticity, and vertical velocity. Given the results of our examination of the reliability of the SDD analyses for the 5 December 1997 vortex, we have concluded that the SDD technique retrieved reliable horizontal wind fields that can be used to examine the structure and evolution of the vortex. Vertical motions were not derived from the SDD wind syntheses because defining adequate lower and/or upper vertical velocity boundary conditions proved difficult given the distance of the vortex from the SDD radar baseline, the lowest operationally collected elevation scan of 0.5°, and the changing convective structure near echo top. However, several derivative quantities calculated from the SDD wind syntheses (i.e., divergence

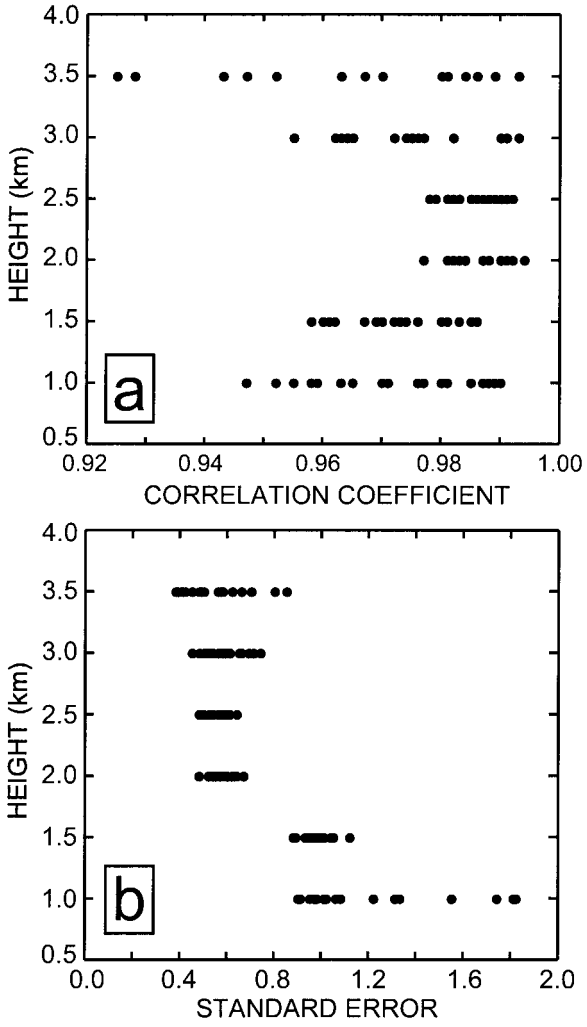

FIG. 7. The (a) correlation coefficients and (b) standard errors from linear least squares analyses for the vortex at 20 syntheses time periods (0853–1203 UTC) within a 125 km × 125 km region.

and vorticity) will be used in section 5 to provide new details about the kinematic structure of winter mesoscale vortices.

4. Great Lakes atmospheric environment

On 4 December 1997, a low pressure center was positioned over northern Lower Michigan and Lake Huron. As the region of low pressure deepened slightly while moving into southern Ontario, Canada, on 5 December 1997, two weak low pressure troughs remained positioned over southern Lake Superior and Lakes Michigan and Huron (Figs. 8a and 8b). These weak troughs likely resulted from the strong atmospheric heating and moistening by each lake, which can hydrostatically reduce the sea level pressure in their vicinity. Pettersen and Calabrese (1959) showed that under strong synoptic flow with similar winter conditions a trough of low pressure can extend through the Great Lake region, while under weaker synoptic flow a center of low pressure can develop in the region.

It is interesting to note that a small-scale 500-hPa absolute vorticity maximum was present in the western Great Lakes region. Figure 9 shows the European Centre for Medium-Range Weather Forecasts (ECMWF) analyses for 0000 and 1200 UTC on 5 December 1997. During this time period the vorticity maximum moved southwestward from northern Lake Michigan to eastern Wisconsin. The positive vorticity advection associated with this 500-hPa feature may have also contributed to the development of the surface pressure troughs and convergence zones in the region. However, it is unclear from the observations whether the small-scale 500-hPa vorticity maximum contributed to the development of the mesoscale vortex. Although Forbes and Merritt (1984) suggested that synoptic-scale forcing (e.g., vorticity advection) is unimportant to vortex formation, it may provide an atmospheric environment (i.e., surface trough, lower-tropospheric convergence, synoptic-scale vertical motions) favorable for mesoscale vortex development.

Figures 8c and 8d show surface air temperatures throughout the western Great Lakes region ranged from $-9°$ to $-1°$C. The Great Lakes were free of ice and surface water temperatures were generally 5°–7°C, based on the satellite-derived surface water temperature analysis of the Great Lakes Environmental Research Laboratory. In the vicinity of Lake Michigan, lake–air temperature differences were 6°–9°C. Previous winter mesoscale vortices have been primarily observed during periods with larger lake–air temperature contrasts. Pease et al. (1988) and Laird (1999) observed mesoscale vortices during time periods having lake–air temperature differences of 10°–15° and 12°–14°C, respectively. Schoenberger (1986a,b) found lake–air temperature differences $>22°$C when multiple meso-γ vortices developed along a land-breeze convergence zone over Lake Michigan. Based on mesoscale model simulations, Hjelmfelt (1990) examined lake–air temperature differences $\leq 18°$C and found the probability for vortex formation over southern Lake Michigan increased with greater lake–air temperature differences. On 5 December 1997, surface total heat fluxes (i.e., combined sensible and latent heat) over central and southeastern Lake Michigan were estimated to be 100–200 W m^{-2} using bulk transfer relationships (e.g., Garratt 1992). These total flux values are near the lower end of typical values observed during winter lake-effect events. For example, Kristovich and Laird (1998) calculated total heat fluxes over Lake Michigan for five widespread lake-effect events during the winter of 1995/96 and found that fluxes ranged from 100 to 700 W m^{-2}. On fewer occasions larger total heat fluxes may occur in the Great Lake region. For example, Sousounis and Fritsch (1994) noted total heat fluxes greater than 1000 W m^{-2} during a lake-aggregate mesoscale event.

Figures 8a and 8b show the surface sea level pressure

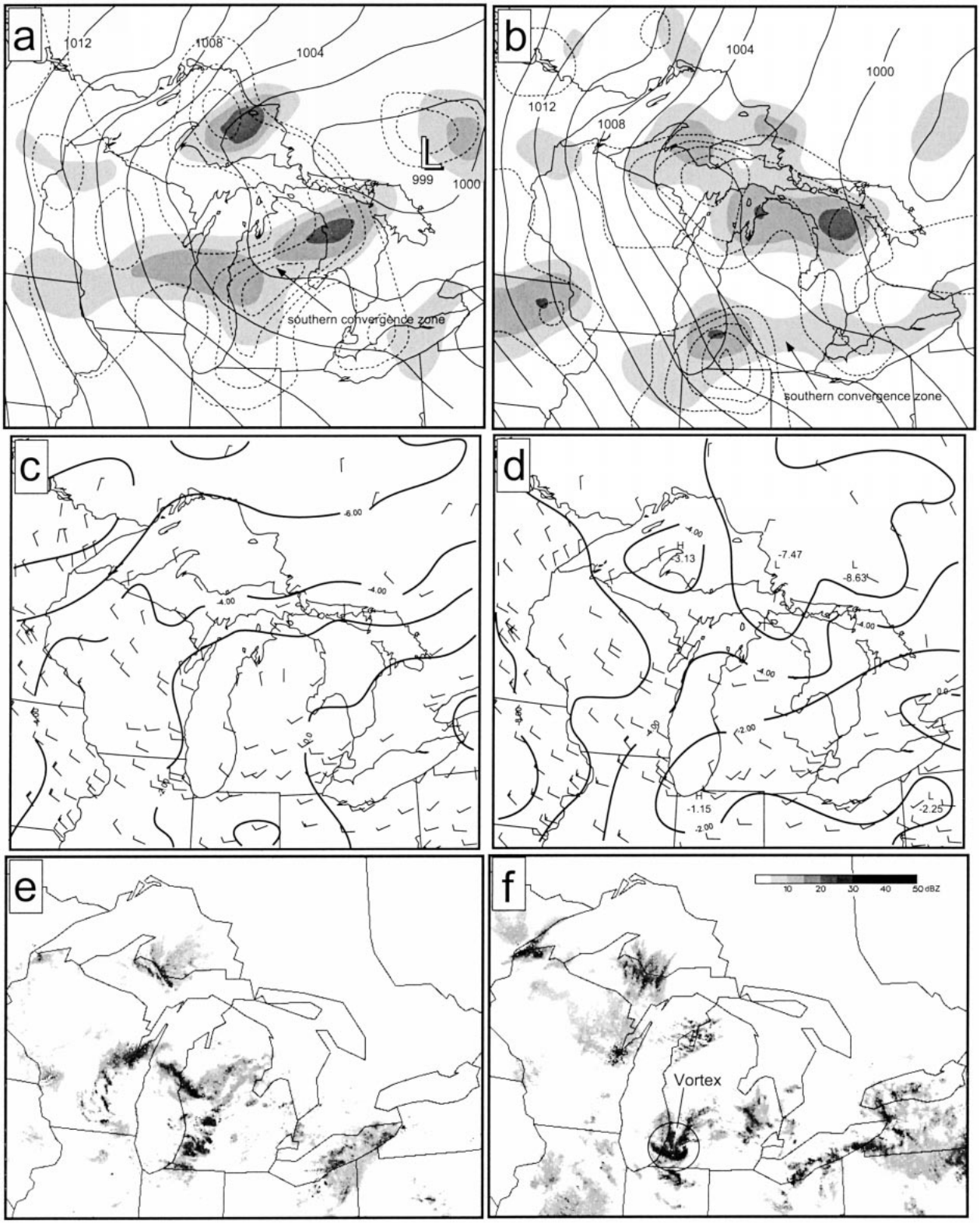

FIG. 8. Near-surface atmospheric conditions at (left column) 0300 UTC and (right column) 1200 UTC on 5 Dec 1997 over the western Great Lakes region. Surface convergence (shaded), positive relative vorticity (dashed lines), and sea level pressure (solid lines) are shown in (a) and (b). Shading of positive convergence begins at 1.0×10^{-5} s^{-1} with an interval of 1.0×10^{-5} s^{-1}. Positive vorticity contouring is the same as convergence. Pressure is contoured every 2 hPa. Surface temperature (contoured every 2°C) and wind (conventional wind barb usage) fields are shown in (c) and (d). Composite radar reflectivity is shown in (e) and (f).

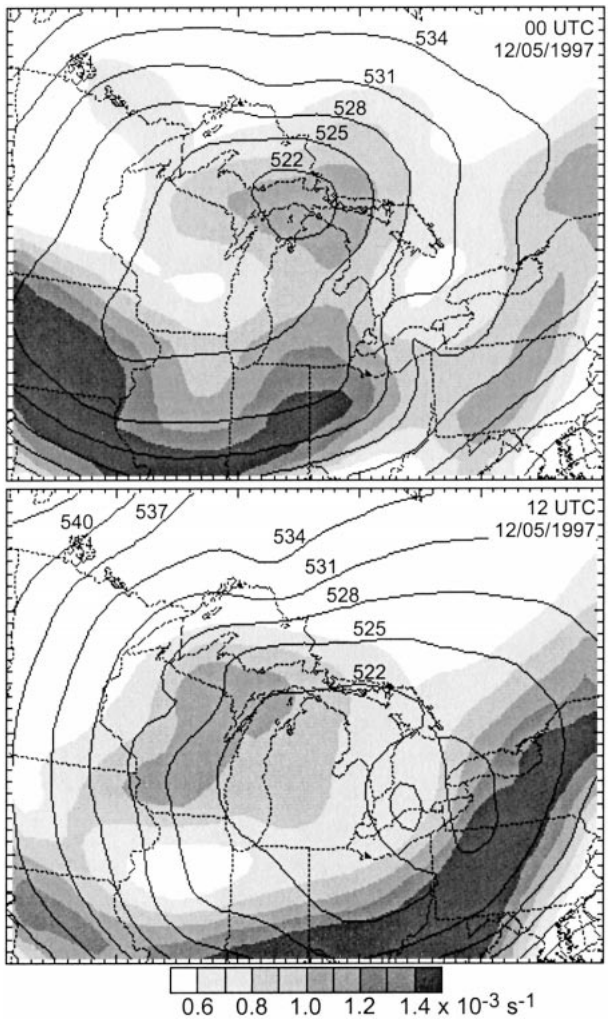

FIG. 9. ECMWF analyses of 500-hPa absolute vorticity (shaded) and height (contour) for (top) 0000 and (bottom) 1200 UTC on 5 Dec 1997. Height contours are shown every 3 dam.

(solid lines), convergence (shaded), and vorticity (dashed lines) fields at 0300 and 1200 UTC on 5 December 1997. Regions of positive surface relative vorticity and convergence, associated with the two trailing troughs, were located over the western Great Lakes region. Figures 8e and 8f show that generally areas of snowfall (i.e., composite radar reflectivity) were located near regions of surface convergence. For example, at 0300 UTC a convergence zone associated with the southern trough was draped across central Lake Michigan and extended into Wisconsin (Fig. 8a). Associated with the synoptic-scale convergence zone, a band of heavier snowfall (i.e., 25–30-dBZ reflectivity) extended westward from western Lower Michigan to Green Bay, Wisconsin (Fig. 8e). The vortex developed over Lake Michigan along this southward-moving convergence zone between 0400 UTC, just prior to a 4-h time period of absent archived Great Lakes composite radar reflectivity data, and 0800 UTC, shortly before it was first observed by KGRR. Unfortunately, available radar, surface, satellite, sounding, and profiler data did not allow for an investigation of the initiation of the vortex or a better determination of the time period of initiation.

Both Forbes and Merritt (1984) and Pease et al. (1988) noted the occurrence and interaction of winter mesoscale vortices with lake-effect convergence zones (e.g., shoreline snowbands). In addition to near-surface convergence, Schoenberger (1986a) described the presence of strong low-level horizontal shear prior to the development of vortices along a land-breeze convergence zone. The surface winds in Fig. 8c and 8d show that cyclonic horizontal shear was present along the southern trough axis and associated convergence zone. Prior to the observations of the vortex by KGRR, the southward-moving convergence zone passed ISS1 and ISS3 at approximately 0600 and 0800 UTC, respectively. The wind profiles retrieved from the ISS 915-MHz Doppler wind profilers were used for a time-to-space conversion to examine the convergent and rotational component of the horizontal shear across the convergence zone. In using this approach, steady-state and along-the-line symmetry are assumed for the convergence zone. Figure 10a shows a horizontal wind shear analysis for ISS1 using the wind components parallel, u', and perpendicular, v', to the trough axis. Pretrough and posttrough wind profiles were used from 0547 and 0647 UTC, respectively, providing winds from near the surface to about 3.5 km. Strong cyclonic shear vorticity (i.e., $du'/ds > 0$) and convergence ($dv'/ds > 0$) were located below 1.5 km, where $ds > 0$ is defined as the posttrough to pretrough direction. A layer of weak divergence was located between 2.5 and 2.9 km and a transition to anticyclonic vorticity occurred above 2.5 km. Figure 10b shows a similar horizontal wind shear analysis for ISS3 using wind profiles from 0747 (pretough) and 0847 (posttrough) UTC. Strong cyclonic vorticity and convergence were confined to below 1.0 km. Weak divergence was present above 1.0 km and minimal cyclonic vorticity was observed above 1.5 km. A schematic of the pretrough and posttrough wind profiles at ISS1 and ISS3 is presented in Figure 11. The pretrough (posttrough) wind profiles at both ISS1 and ISS3 show a veering (backing) of the wind with height associated with warm-air (cold air) advection. This is generally consistent with the surface temperature and wind fields shown in Figs. 8c and 8d.

The eastern portion of the southward-moving convergence zone that passed over ISS3 had structural similarities to the section that moved over ISS1, 120 km to the west-northwest 2 h earlier. However, the eastern section of the convergence zone was shallower and had weaker low-level convergence. At both ISS1 and ISS3 during the convergence zone passage, the cyclonic vorticity was 2.6×10^{-4} s^{-1} at 500 m. This value is comparable to relative vorticity values found by Miller et al. (1996), $2–8 \times 10^{-4}$ s^{-1}, for an arctic cold front when using an array of surface mesonet station separated by

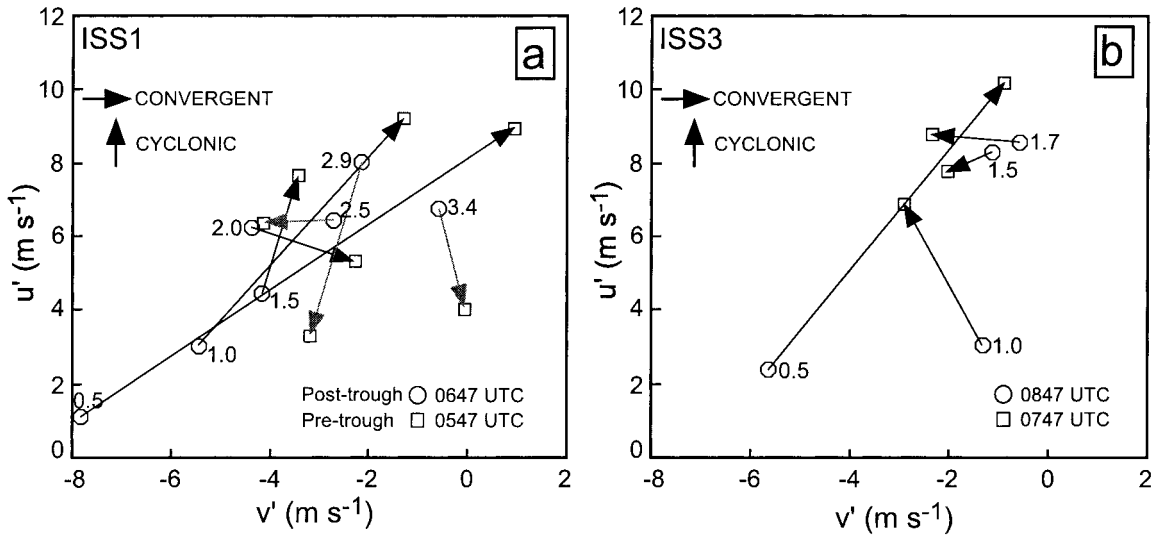

FIG. 10. Horizontal shear analyses for (a) ISS1 and (b) ISS3 as the synoptic trough axis and associated convergence zone passed each site. Analyses show convergence zone parallel, u', and perpendicular, v', wind components. Numbers represent the height (km) of the winds used. Analyses above 2.5 km are shaded gray.

15–25 km. The 500-m convergence was stronger over western Michigan, 2.9×10^{-4} s^{-1} for ISS1, and weaker over central Michigan, 1.6×10^{-4} s^{-1} for ISS3, resulting in deeper precipitation echoes to the west near the Lake Michigan shoreline.

Several previous investigations (e.g., Pease et al. 1988; Laird 1999) have shown that during the occurrence of winter mesoscale vortices the atmospheric static stability in the Great Lakes region is nearly neutral ($d\theta/dz$) = 0.5°–1.5°C km^{-1}) below 2.0 km. The ISS1 and ISS3 soundings released at 0600 UTC over western Michigan exhibited a deep layer of conditional static stability (generally $d\theta/dz < 4.0$°C km^{-1}) from the surface to about 620 hPa. Figure 12 shows the 0600 UTC sounding that was launched as the convergence zone and associated snowband were passing over ISS1. A layer of nearly neutral static stability was present from near the surface to about 1.4 km. Stability analysis of the 0600 UTC ISS1 sounding shows a region of positive convective available potential energy from 0.5 to 1.4 km resulting in a calculated upward motion of approximately 4.2 m s^{-1} at 1.4 km.

The synoptic and mesoscale atmospheric environments provided favorable conditions for the development of the winter mesoscale vortex on 5 December 1997. Organized convergence was observed over Lake Michigan prior to vortex formation (i.e., synoptic trough) and the lower atmosphere (<1.4 km) had nearly neutral static stability, similar to previous investigations (e.g., Forbes and Merritt 1984, Laird 1999). However, it is interesting to note that total surface heat fluxes were lower than typically observed during winter lake-effect events. Therefore, the likely less significant contribution of the smaller lake–air temperature differences and weaker surface fluxes to the development and maintenance of the vortex may have been partially counterbalanced by the presence of the well-organized low-level convergence zone and weak stability in the lower troposphere.

5. Mesoscale vortex structure and evolution

The vortex was first observed by the KGRR radar over Lake Michigan at approximately 0830 UTC in association with the weak trough and convergence zone oriented southwest to northeast across Lakes Michigan and Huron. The vortex moved onshore and propagated toward the southeast (Fig. 1) as the trough axis rotated cyclonically about a low pressure center moving northeastward over Quebec, Canada. Based on radar reflectivity fields and the analysis shown in Fig. 5, the vortex intensity and structure did not appear to substantially decrease after moving onshore around 1000 UTC and inland during the following 2 h (vortex track shown in Fig. 1).

A decrease in the vortex intensity may have been expected due to increased surface roughness after coming onshore and the reduction of surface heat and moisture fluxes after moving away from Lake Michigan. Since a substantial decrease in intensity did not occur and Lake Michigan total surface fluxes were relatively weak (100–200 W m^{-2}), the vortex was likely linked closely with favorable dynamic conditions, such as horizontal shear (Figs. 10 and 11) and vertical motions, along the synoptic trough and convergence zone.

Although the ISS1 sounding shown in Fig. 12 does not show a near-surface stable layer, several soundings launched during 5 December over Lower Michigan (not shown) suggested a shallow near-surface stable layer was present. The presence of a stable internal boundary

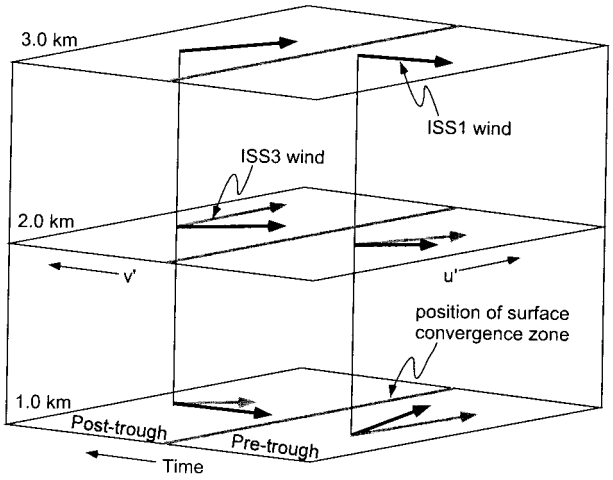

FIG. 11. Schematic of the pre- and posttrough wind profiles at ISS1 and ISS3. Winds at the 1.0-, 2.0-, and 3.0-km levels are composed of the trough axis parallel, u', and perpendicular, v', wind components. Black and gray winds represent ISS1 and ISS3 winds, respectively. The position of the surface convergence zone is shown on all three levels by the thick gray line.

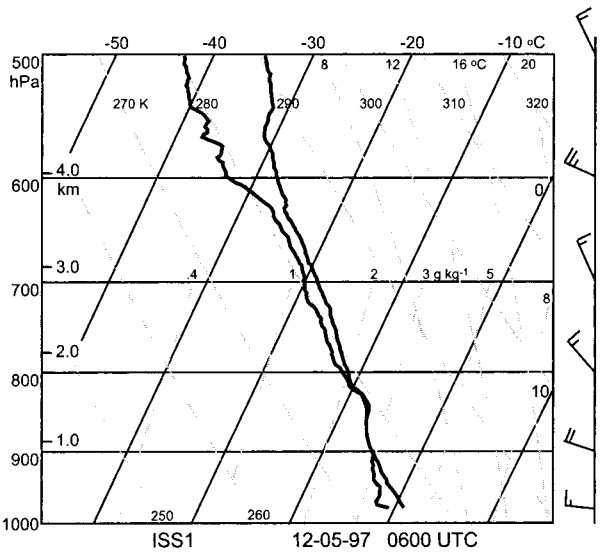

FIG. 12. The 0600 UTC ISS1 sounding on 5 Dec 1997.

layer over land may have resulted in a decoupling from the surface of the convective boundary layer that had developed over Lake Michigan. This situation would result in reduced fricitional influences on the vortex as it moved inland.

The 2-km radar reflectivity fields in Fig. 13 show the vortex had a pronounced asymmetric convective structure and at least three well-defined radial convective bands, where regions of heavier snowfall were located. As seen from a comparison of the upper and lower panels in Fig. 13, these radial snowbands slowly rotated about the vortex center at <1.0 m s^{-1}. During the evolution of the vortex, a distinct weak-reflectivity region or ''eye'' formed near the center of the circulation. The weak-reflectivity region was present for nearly 2.5 h suggesting that the vortex circulation may have contained a local region of subsidence near the center. The convection associated with the vortex remained relatively shallow, with the echo tops only reaching heights of approximately 4.5 km. However, the height of the convection associated with the vortex was greater than that of typical lake-effect systems, which are generally below 3 km (e.g., Braham 1983; Kristovich 1993).

The vortex circulation on 5 December 1997 was composed of a combination of rotation on the meso-β scale and convergence on the meso-γ scale associated with the embedded radial snowbands. The SDD relative-wind and convergence fields are shown with the reflectivity field at 1013, 1043, and 1113 UTC in Fig. 13. All variables are shown at the 2-km level. The SDD relative-wind and convergence fields exhibit a temporally coherent evolution during the 1-h time period. Several features of the SDD wind and convergence fields appear closely associated with coherent structures in the 2-km reflectivity field. The cyclonic circulation in the relative wind fields is clearly visible and its center is nearly collocated with the weak reflectivity region at the focus of the three radial snowbands. The most intense radial band, the southernmost band that reached a height of just over 4.5 km, contained reflectivities of nearly 32 dBZ. Figure 13 shows inflow into the southernmost band at 2 km. An area of strong convergence ($\sim 7.5 \times 10^{-4}$ s^{-1}) is collocated with the position of the southern radial snowband in the reflectivity fields in Figs. 13b, 13d, and 13f. The two northern bands are shallower and during the 1-h time period show evidence of weak outflow and increased divergence at 2 km. At 1013 UTC (Figs. 13a,b), outflow and divergence are also associated with the shallow weak-reflectivity band to the south of the vortex. Several of these features are also evident in Fig. 14.

Figure 14 shows the vertical structure of the vortex at 1053 UTC. The SDD relative-wind and convergence fields are shown with the reflectivity field from the 1.0- to 4.0-km levels. Convergent flow into the lower portion of the vortex is apparent in Figs. 14a–d and shows convergence values of $\geq 5.0 \times 10^{-4}$ s^{-1}. Figure 14c clearly shows the cyclonic low-level circulation. Nearly the entire region of the vortex at 1.5 km, especially in the vicinity of the higher-reflectivity snowbands, is convergent except for a small area of weak divergence (i.e., $\sim 2.5 \times 10^{-4}$ s^{-1}) near the vortex center. This localized region of low-level divergence near the weak-reflectivity vortex center is further evidence that a region of subsidence existed at this location. Above 2.5 km, relative winds show outflow from the vortex center and the convergence fields show increased divergence with altitude. Above 3.5 km nearly the entire region of the SDD analysis is divergent, including the area in the vicinity of the deeper southern radial snowband (Figs. 14m,n).

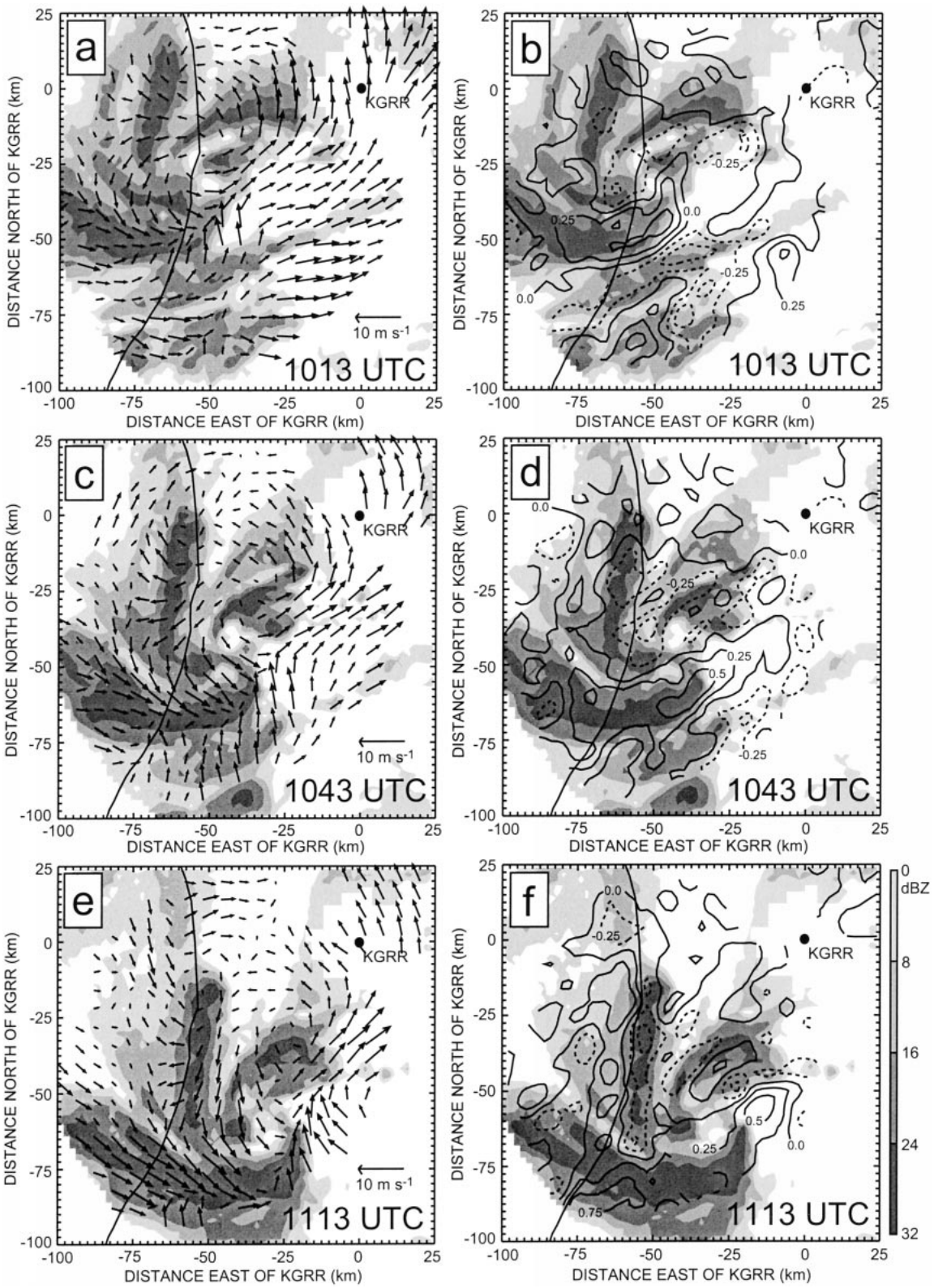

FIG. 13. Radar reflectivity (shaded), SDD relative winds (left column), and convergence (right column) shown at the 2-km level for (a)–(b) 1013, (c)–(d) 1043, and (e)–(f) 1113 UTC. Convergence is contoured at 0.25×10^{-3} s^{-1} intervals. Solid lines represent convergence and dashed lines divergence. The location of Lake Michigan shoreline is shown by thick solid line.

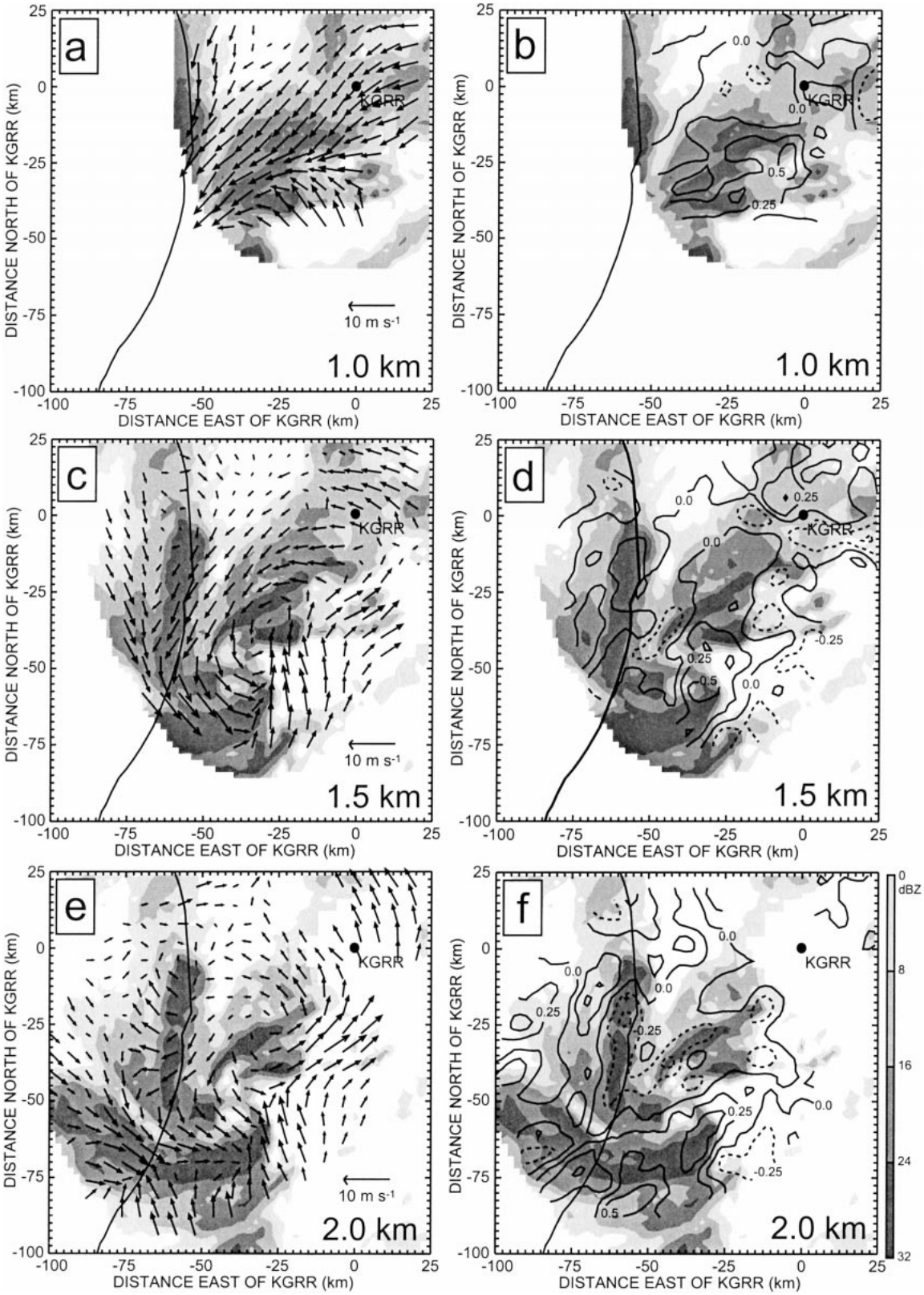

FIG. 14. Radar reflectivity (shaded), SDD perturbation winds (left column), and convergence (right column) shown at 1053 UTC for (a)–(b) 1.0 km, (c)–(d) 1.5, (e)–(f) 2.0, (g)–(h) 2.5, (i)–(j) 3.0, (k)–(l) 3.5, and (m)–(n) 4.0 km. Convergence is contoured at 0.25×10^{-3} s^{-1} intervals. Solid lines represent convergence and dashed lines divergence. The location of Lake Michigan shoreline is shown by thick solid line.

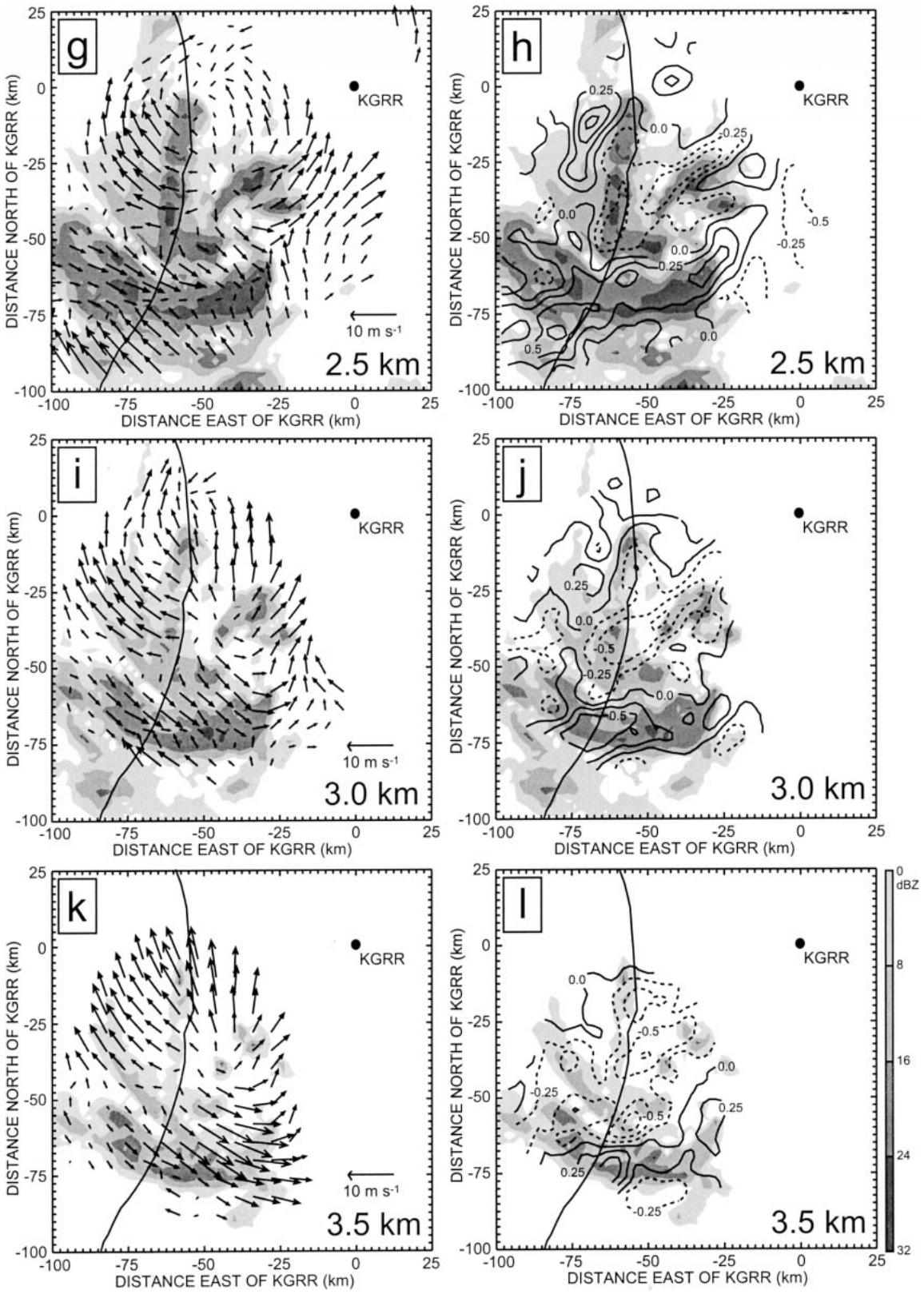

FIG. 14. (*Continued*)

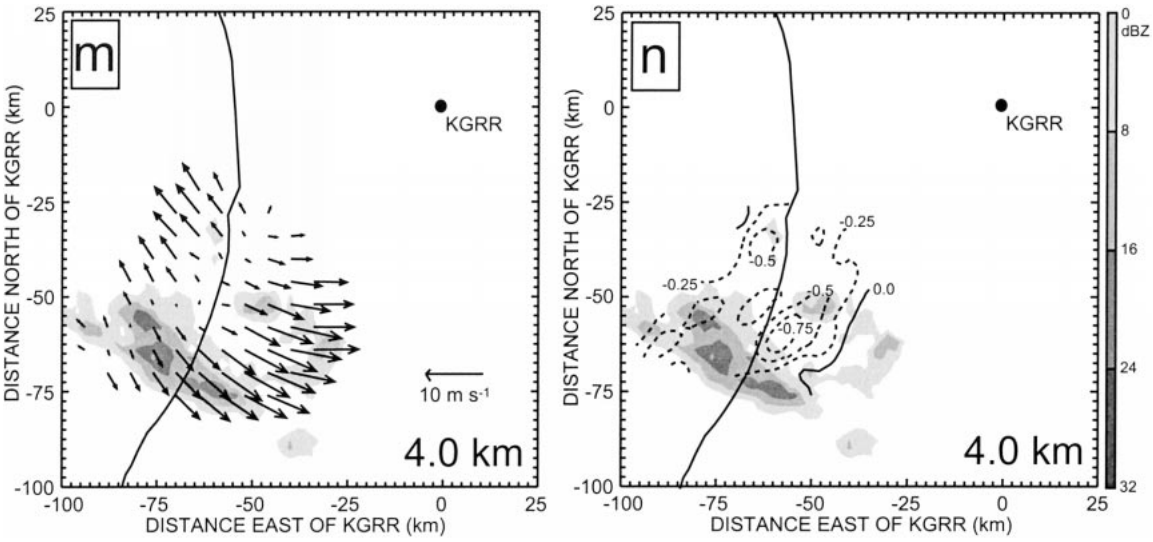

FIG. 14. (*Continued*)

Although Schoenberger (1986a) described vortices that had a smaller horizontal scale (~10 km diameter) and were shallower (~2 km depth) than our vortex, there are some similarities in their structure. Schoenberger (1986a) found several of the vortices developed a weak-reflectivity region or eye at their centers and had maximum 1-km level convergence and relative vorticity values of 3.8×10^{-3} s^{-1} and 6.0×10^{-3} s^{-1}, respectively. He found the strongest convergence was confined to the lowest 0.4 km above the surface and the strong cyclonic circulation of the vortices was present near the upper levels of the snowband (~2 km level) even though this portion of the band was increasingly divergent.

Figure 15 shows vertical profiles of area-averaged convergence and vorticity for five SDD analyses covering a 2-h time period (0943–1143 UTC). Convergence and vorticity were averaged at each 0.5-km interpolated level within a 30 km × 30 km region centered on the low-level cyclonic vortex circulation. The lowest level included in this analysis was 1.5 km due to the distance of the vortex from KGRR and the lowest available elevation scan of 0.5°. The average convergence profile (thick black line) in Fig. 15a shows weak convergence at 1.5 km, a transition to divergence between 1.5 and 2.0 km, and increasing divergence with height to 4.0 km. The average relative vorticity profile (thick black line) in Fig. 15b exhibits strong positive relative vorticity at 1.5 km with an average value of 2.9×10^{-4} s^{-1} and decreases rapidly with height to a value of 0.7×10^{-4} s^{-1} at 4.0 km. These convergence and vorticity profiles represent the region within the core of the vortex circulation. Profiles examined within several different radial snowbands were more variable. For example, Fig. 14 shows convergence present to 3.5 km with the deeper southern band, and a transition near the 2-km level from low-level convergence to divergence in the two northern bands.

Although no thermodynamic data (surface or sounding) were available within the vortex, both the area-averaged convergence and vorticity profiles near the vortex core can be used to provide information about the thermodynamic character of the circulation. The decrease of relative vorticity with height suggests that the vortex was likely a warm-core system, similar to both tropical cyclones and polar lows (e.g., Rasmussen 1989). Figure 16 shows a conceptual model of the three-dimensional flow and thermodynamic environment associated with the cyclonic vortex. The presence of a warm-core cyclonic vortex would hydrostatically reduce the pressure near the surface resulting in an increase of relative vorticity due to Coriolis deflection of the convergent low-level flow. At higher levels in the cyclonic vortex circulation, pressure would be increased relative to the surrounding environment and a decrease in relative vorticity at these levels would occur. The profiles of area-averaged convergence and vorticity, shown in Fig. 15, and the SDD relative-wind and convergence fields, shown in Fig. 14, support this simplified conceptual model of the 5 December 1997 winter mesoscale vortex and provide evidence the vortex was a warm-core system.

6. Summary and conclusions

During the early morning hours of 5 December 1997, a winter mesoscale vortex was observed over Lake Michigan and southwestern Lower Michigan. As the vortex propagated inland, there were rapid increases in the snowfall intensity over the region. This article examines the kinematic structure and evolution of this vortex. The synthetic dual-Doppler technique was used to determine the horizontal wind field from single-Doppler radial velocity measurements collected by the National Weather Service's Grand Rapids, Michigan WSR-88D radar.

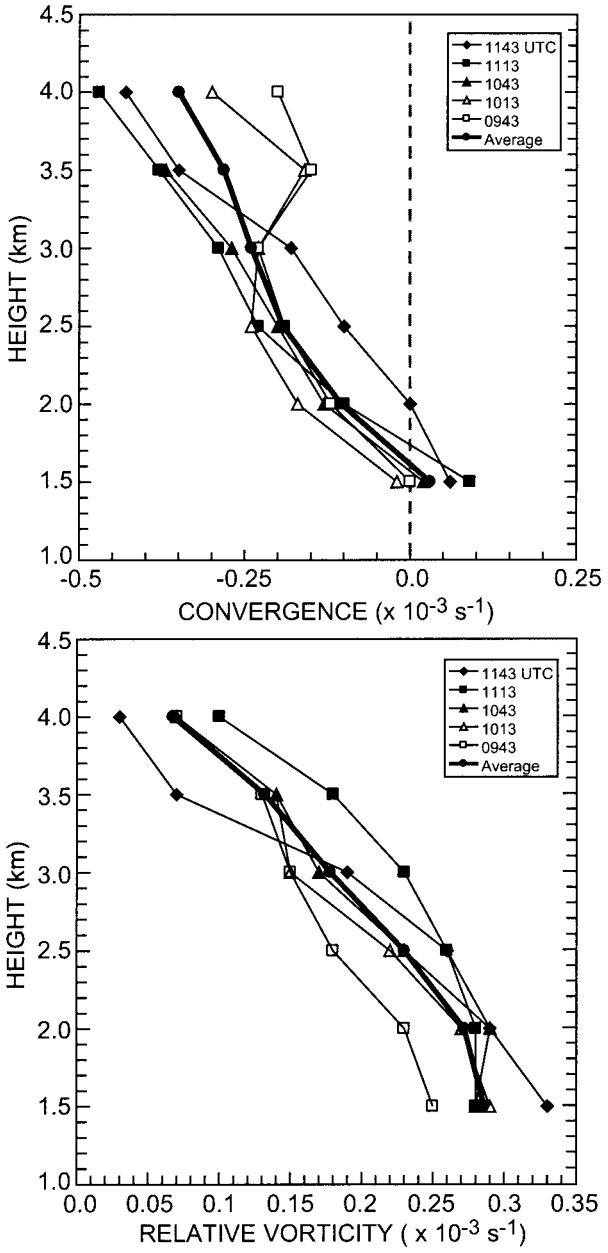

FIG. 15. Vertical profiles of (a) area-averaged convergence and (b) relative vorticity for five SDD analyses covering a 2-h time period (0943–1143 UTC). The averaged convergence and vorticity values were calculated from data within a 30 km × 30 km region centered on the low-level cyclonic vortex circulation at each time period. Average profiles are shown by thick solid line.

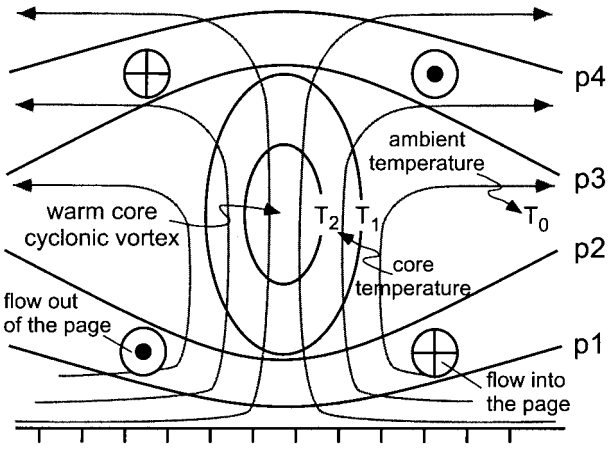

FIG. 16. A conceptual model of the three-dimensional flow and thermodynamic environment associated with the cyclonic winter mesoscale vortex. Shaded area denotes warm vortex core. Solid black lines represent constant pressure surfaces. Vertical circulation is shown by solid gray lines and areas of flow into and out of the page are labeled.

The absence of data over Lake Michigan for this event made the mechanisms responsible for the initiation of the vortex impossible to determine. Nevertheless, some inferences can be made. Previous investigations of wintertime mesoscale vortices in the Great Lakes region (e.g., Forbes and Merritt 1984; Laird 1999) have described the atmospheric conditions favorable for their development. These include 1) a weak synoptic pressure gradient and low wind speeds, 2) large lake–air temperature differences, 3) low atmospheric stability, and 4) organized convergence over the lake. Several of these conditions were present during the 5 December 1997 vortex event, such as low static stability and organized convergence over Lake Michigan. However, surface sensible and latent heat fluxes were small and only moderate lake–air temperature differences of 6°–9°C were observed over Lake Michigan, suggesting that dynamic conditions, such as horizontal shear across the trough axis and associated convergence zone, were more important than topographic/thermal forcing (Pease et al. 1988) for the development of the vortex. Mesoscale modeling and detailed observational studies are being conducted to further examine the initiation mechanisms, structure, and evolution of winter mesoscale vortices and the atmospheric conditions under which they develop.

The radar reflectivity fields showed the vortex had a pronounced asymmetric convective structure and at least three well-defined radial convective bands where regions of heavier snowfall were located. During the evolution of the vortex, a distinct weak-reflectivity region or eye formed near the center of the circulation suggesting that a small-scale region of subsidence may have been present. The SDD results showed the vortex circulation was composed of a combination of rotation on the meso-β scale and convergence on the meso-γ scale associated with the embedded radial snowbands. Several features of the SDD wind and convergence fields were closely tied to coherent structures in the reflectivity field. Virtually the entire region of the vortex at 1.5 km, especially in the vicinity of the higher-reflectivity snowbands, was convergent except for a small area of weak divergence near the vortex center. Above 2.5 km, perturbation winds showed outflow from the vortex center

and the convergence fields showed an increased region of divergence with altitude. At 4.0 km nearly the entire region of the SDD analysis was divergent. Profiles of SDD convergence showed weak convergence at 1.5 km, a transition to divergence between 1.5 and 2.0 km, and increasing divergence with height to 4.0 km. It was found from SDD relative vorticity profiles that strong positive relative vorticity existed at 1.5 km and decreased rapidly with height to 4.0 km. The profiles of area-averaged convergence and vorticity and the SDD relative wind and convergence fields support the simplified conceptual model, shown in Fig. 16, of the 5 December 1997 vortex and provide evidence the vortex was a warm-core system, similar to both tropical cyclones and polar lows.

The analyses presented in this article provide further support for the use of the SDD technique to examine mesoscale events, provided the limiting aspect of the technique are adequately examined and satisfied. The results from this investigation also show that the SDD technique can recover meaningful derived parameters, such as convergence and vorticity in some situations. While this case study successfully used the SDD technique to gain a better understanding of a mesoscale event, it is still unclear whether this method can regularly be used to successfully retrieve horizontal wind fields in a variety of situations. Further investigations should be conducted to objectively compare SDD results to other single-Doppler retrieval methods (e.g., Tuttle and Foote 1990; Sun and Crook 1994) for a diverse array of mesoscale events.

Acknowledgments. We thank Robert Rauber and John Walsh for suggestions and comments on this investigation and an early version of the manuscript. The authors would like to especially thank Sherrie Fredrick of NCAR/MMM for her work on SPRINT and CEDRIC. We are grateful to both Brian Jewett and David Wojtowicz of the Department of Atmospheric Sciences at the University of Illinois for making available objective analysis code and archived data. In addition, Greg Stossmeister of NCAR/JOSS was helpful in obtaining the WSR-88D archived data collected during Lake-ICE. This research was supported under National Science Foundation Grants ATM-9510098 and ATM-9816306.

REFERENCES

Bluestein, H. B., and D. S. Hazen, 1989: Doppler-radar analysis of a tropical cyclone over land: Hurricane Alicia (1983) in Oklahoma. *Mon. Wea. Rev.,* **117,** 2594–2611.

——, S. D. Hrebenach, and E. A. Brandes, 1991: A test of the synthetic dual-Doppler analyses technique: Two case studies. Preprints, *25th Int. Conf. on Radar Meteorology,* Paris, France, Amer. Meteor. Soc., 634–637.

——, ——, C.-F. Chang, and E. A. Brandes, 1994: Synthetic dual-Doppler analysis of mesoscale convective systems. *Mon. Wea. Rev.,* **122,** 2105–2124.

Braham, R. R., Jr., 1983: The Midwest snow storm of 8–11 December 1977. *Mon. Wea. Rev.,* **111,** 253–272.

Crum, T. D., R. L. Alberty, and D. W. Burgess, 1993: Recording, archiving, and using WSR-88D data. *Bull. Amer. Meteor. Soc.,* **74,** 645–653.

Doviak, R. J., P. S. Ray, R. G. Strauch, and L. J. Miller, 1976: Error estimation in wind fields drived from dual-Doppler radar measurements. *J. Appl. Meteor.,* **15,** 868–878.

Forbes, G. S., and J. M. Merritt, 1984: Mesoscale vortices over the Great Lakes in wintertime. *Mon. Wea. Rev.,* **112,** 377–381.

Gal-Chen, T., 1982: Errors in fixed and moving frames of reference: Applications for conventional and Doppler radar analysis. *J. Atmos. Sci.,* **39,** 2279–2300.

Garratt, J. R., 1992: *The Atmospheric Boundary Layer.* Cambridge University Press, 316 pp.

Hjelmfelt, M. R., 1990: Numerical study of the influence of environmental conditions on lake-effect snowstorms over Lake Michigan. *Mon. Wea. Rev.,* **118,** 138–150.

Klimowski, B. A., and J. D. Marwitz, 1992: The synthetic dual-Doppler analysis technique. *J. Atmos. Oceanic Technol.,* **9,** 728–745.

Kraus, M. J., 1974: Doppler radar investigation of flow patterns within thunderstorms. Environmental Research Paper 481, AFCRL-TR-74-0290, 86 pp. [Available from Air Force Cambridge Research Laboratories, Hanscom AFB, MA 61731.]

Kristovich, D. A. R., 1993: Mean circulations of boundary-layer rolls in lake-effect snow storms. *Bound.-Layer Meteor.,* **63,** 293–315.

——, and N. F. Laird, 1998: Observations of widespread lake effect cloudiness: Influences of lake surface temperature and upwind conditions. *Wea. Forecasting,* **13,** 811–821.

——, and Coauthors, 2000: The Lake-Induced Convection Experiment (Lake-ICE) and the Snowband Dynamics Project. *Bull. Amer. Meteor. Soc.,* **81,** 519–554.

Laird, N. F., 1999: Observation of coexisting mesoscale lake-effect vortices over the western Great Lakes. *Mon. Wea. Rev.,* **127,** 1137–1141.

Lhermitte, R. M., and L. J. Miller, 1970: Doppler radar methodology or the observation of convective storms. Preprints, *14th Conf. on Radar Meteorology,* Tuscon, AZ, Amer. Meteor. Soc., 133–138.

Miller, L. J., and R. A. Kropfli, 1980: The multiple Doppler radar workshop. Part II: Experimental design and procedures. *Bull. Amer. Meteor. Soc.,* **61,** 1173–1177.

——, C. G. Mohr, and A. J. Weinheimer, 1986: The simple rectification of Cartesian space of folded radial velocities from Doppler radar sampling. *J. Atmos. Oceanic Technol.,* **3,** 162–174.

——, J. D. Tuttle, and G. B. Foote, 1990: Precipitation production in a large Montana hailstorm: Airflow and particle growth trajectories. *J. Atmos. Sci.,* **47,** 1619–1646.

——, M. A. LeMone, W. Blumen, R. L. Grossman, N. Gamage, and R. J. Zamora, 1996: The low-level structure and evolution of a dry arctic front over the central United States. Part I: Mesoscale observations. *Mon. Wea. Rev.,* **124,** 1648–1675.

Mohr, C. G., and R. L. Vaughan, 1979: An economical procedure for Cartesian interpolation and display of reflectivity data in three-dimensional space. *J. Appl. Meteor.,* **18,** 661–670.

——, L. J. Miller, R. L. Vaughan, and H. W. Frank, 1986: The merger of mesoscale datasets into a common Cartesian format for efficient and systematic analyses. *J. Atmos. Oceanic Technol.,* **3,** 144–161.

Peace, R. L., Jr., 1966: Radar characteristics of lake-effect storms. *Proc. 12th Conf. on Radar Meteorology,* Norman, OK, Amer. Meteor. Soc., 454–460.

——, R. A. Brown, and H. G. Camnitz, 1969: Horizontal motion field observations with a single pulse Doppler radar. *J. Atmos. Sci.,* **26,** 1096–1103.

Pease, S. R., W. A. Lyons, C. S. Keen, and M. R. Hjelmfelt, 1988: Mesoscale spiral vortex embedded within a Lake Michigan snow squall band: High resolution satellite observations and numerical model simulations. *Mon. Wea. Rev.,* **116,** 1374–1380.

Petterssen, S., and P. A. Calabrese, 1959: On some weather influences

due to warming of the air by the Great Lakes in winter. *J. Meteor.*, **16,** 646–652.

Pitts, D. E., J. T. Lee, J. Fein, Y. Sasaki, K. Wagner, and R. Johnson, 1977: Mesoscale cloud features observed from Skylab. Skylab Explores the Earth, NASA-SP-80, 479–501.

Rasmussen, E. A., 1989: A comparative study of tropical cyclones and polar lows. *Polar and Arctic Lows,* P. F. Twitchell, E. Rasmussen, and K. L. Davidson, Eds., A. Deepak Publishing, 47–80.

Schoenberger, L. M., 1986a: Mesoscale features of a midlake snow band. Preprints, *23d Conf. on Radar Meteorology,* Snowmass, CO, Amer. Meteor. Soc., JP206–JP209.

——, 1986b: Mesoscale features of the Michigan land breeze using PAM II temperature data. *Wea. Forecasting,* **1,** 127–135.

Sheffield, R. K., 1964: A series of mesolows associated with a Lake Erie snowstorm. WSR 57 Radar Program Progress Rep. 14, USWB, 34–38. [Available from National Weather Service Eastern Region, Scientific Services Division, 630 Johnson Avenue, Bohemia, NY 11716.]

Sousounis, P. J., and J. M. Fritsch, 1994: Lake aggregate mesoscale disturbances. Part II: A case study of the effects on regional and synoptic-scale weather systems. *Bull. Amer. Meteor. Soc.,* **75,** 1793–1811.

Sun, J., and A. Crook, 1994: Wind and thermodynamic retrieval from single-Doppler measurements of a gust front observed during Phoenix II. *Mon. Wea. Rev.,* **122,** 1075–1091.

Tuttle, J. D., and G. B. Foote, 1990: Determination of the boundary layer airflow from a single Doppler radar. *J. Atmos. Oceanic Technol.,* **7,** 218–232.